

Time-Dependent Density Functional Theory Study of the Electronic Excitation Spectra of Chlorophyllide *a* and Pheophorbide *a* in Solvents

Zheng-wang Qu,* Hui Zhu, and Volkhard May*

Humboldt Universität zu Berlin, Institut für Physik, AG Photobiophysik, Newtonstrasse 15, D-12489 Berlin, Germany

Reinhard Schinke†

Max-Planck-Institut für Dynamik and Selbstorganisation, Bunsenstrasse 10, D-37073 Göttingen, Germany

Received: July 2, 2008; Revised Manuscript Received: November 5, 2008

The electronic excitation spectra of both chlorophyllide *a* (Chl) and pheophorbide *a* (Pheo) molecules in solvents have been investigated by using the time-dependent density functional theory (TDDFT) along with the polarizable continuum solvation model (PCM). With increasing Hartree–Fock (HF) exchange percentage in DFT functionals, the predicted HOMO–LUMO gaps increase linearly while the excitation energies increase gradually and even strongly for excited states with partial intramolecular charge-transfer (CT) nature. On the basis of the calculated excitation energies, oscillator strengths and frontier molecular orbital analysis, we provide some new insights into the absorption spectra of Pheo and Chl both in the gas phase and in solutions, especially for the B and higher electronic absorption bands. It is shown that the experimental observed visible Q_y and Q_x and ultraviolet B_y and B_x bands are all due to singlet $^1(\pi,\pi^*)$ valence excitations, with the B bands being more strongly red-shifted by solvent effects. Two $^1(\pi,\pi^*)$ dark states are predicted slightly below (or near) the strong B band for both Chl and Pheo, with one related to the excitation of tetrapyrrole ring and the other related to the excitation of ring I vinyl substituent. The $^1(n,\pi^*)$ CT state from the conjugated carbonyl substituent is above B bands and further strongly blue-shifted by solvent effects. The higher η and N bands are mainly due to $^1(\pi,\pi^*)$ valence excitations with only partial CT character, which are also red-shifted in solvent.

1. Introduction

Pheophorbide *a* (Pheo, $C_{35}H_{36}N_4O_5$) and chlorophyllide *a* (Chl, $C_{35}H_{34}MgN_4O_5$) (see Figure 1) are vital pigments for photosynthesis¹ and have also found many potential applications such as photodynamic therapy of cancer tumor based on their excited states.² Both molecules contain a planar tetrapyrrole macrocycle (rings I–IV) and an additional ring V next to III, with various substituents reducing the molecular symmetry. Due to their central role in both photosynthetic and photodynamic therapy processes, the excited states of Pheo and Chl have attracted a lot of experimental^{2–9} and theoretical interests.^{10–18}

For Pheo and Chl molecules, the experimentally observed visible Q bands and near-ultraviolet B bands are usually interpreted in terms of the Gouterman four-orbital model^{19,20} involving mainly single-excitation transitions from two highest occupied molecular orbital (HOMO) into two lowest unoccupied molecular orbital (LUMO). However, due to their low molecular symmetry, reliable ab initio calculations are significantly challenging. The Gouterman model is supported by recent SAC-CI calculations with four reference configurations,¹⁰ while TDDFT and MRCI/DFT studies^{11–17} show that such a model is valid only for the visible Q bands, since additional dark states are found between the Q and B bands and higher excitation configurations (rather than only singles) are also important for B band transitions. However, the nature of possible dark states

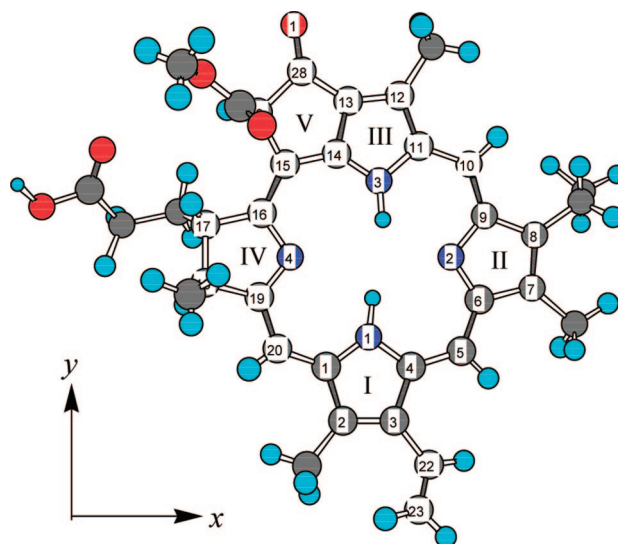


Figure 1. Molecular structure of pheophorbide *a* (Pheo, $C_{35}H_{36}N_4O_5$) placed in the Cartesian x – y plane with the N, C, H, and O atoms shown as blue, gray, cyan, and red spheres, respectively. The N4→N2 direction is chosen as the x -axis, and five conjugated rings (I up to V) and some atomic labels are shown. In the corresponding structure of chlorophyllide *a* (Chl, $MgC_{35}H_{34}N_4O_5$), two central H atoms should be replaced by an Mg atom.

between Q and B bands and of higher (η_1 , η_2 , and N) absorption bands is still elusive due to the possible failure of time-dependent density functional theory (TDDFT) method for excited states

* To whom correspondence should be addressed. E-mail: zheng@physik.hu-berlin.de (Z.Q.); may@physik.hu-berlin.de (V.M.).

† E-mail: rschink@gwdg.de.

of charge-transfer (CT) character,^{21,22} for which the excitation energy could be seriously underestimated especially when pure DFT functionals are used.^{12,13,15} Inclusion of nonlocal Hartree–Fock (HF) exchange into hybrid DFT functionals is suggested as an efficient way to overcome such problem.^{13,15,22}

In this paper, we will present detailed theoretical analysis of and provide new insights into the electronic absorption spectra of both Pheo and Chl molecules both in the gas phase and in solution, especially for the B band and higher bands. This work is also motivated by the recent interests on the exciton dynamics and spectra of flexible chromophore complexes of Pheo in solvents in our group.^{23–25} Moreover, since available experimental spectra for Pheo and Chl are obtained in solutions,^{2,3,8,9} solvent effects should also be taken into account for more realistic comparison between theory and experiment. For Chl molecule, the coordination of explicit solvent molecule to the central Mg-ion will be considered. A comparison between the calculated Chl and Pheo spectra can be helpful for understanding the subtle effects of central Mg coordination on photophysical properties of similar porphyrin molecules.

2. Computational Details

All calculations are done using the GAUSSIAN 03 program.²⁶ The Becke's three-parameter exchange functional²⁷ along with the Lee–Yang–Parr's correlation functional (B3LYP)²⁸ and the standard split-valence plus polarization function 6-31G(d,p) basis set^{29,30} are chosen for the singlet ground-state geometry optimization. This leads to 840 and 849 basis functions with 1484 and 1522 primitive gaussians for Pheo and Chl molecules, respectively. The fully optimized stationary points are further characterized by harmonic vibrational frequency analysis to ensure that real local minima are found without any imaginary vibrational frequency. To test the effects of electron correlation on the ground-state geometries, the Pheo geometries are also optimized at the HF/6-31G(d,p) level³¹ of theory and compared with the available X-ray crystal structure of methyl pheophorbide *a*.⁶ To account for the effects of solvent–Mg coordination and explicit H-bonding to ring V carbonyl substituent, solvent complexes of Pheo and Chl with one or two explicit solvent molecules are also optimized at the B3LYP/6-31G(d,p) level of theory.

Time-dependent^{32,33} (TD) B3LYP calculations are performed for the lowest 15 singlet excited states with larger 6-31+G(d,p) basis set including diffuse function³⁴ for more reliable description of excited-state wave functions. The hybrid B3LYP functional (with 20% HF exchange) is chosen here because nonlocal HF exchange within DFT functional may be helpful to overcome the problem of low-lying spurious charge-transfer (CT) states from pure GGA functionals such as BP86 (with 0% HF exchange).³⁵ Further calculations using the semiempirical ZINDO (INDO/S CIS; with 100% HF exchange) method³⁶ are also performed, which may further cure the problem of CT states and is more accurate than traditional *ab initio* CIS method³⁷ due to the use of parameters fitting to experimental data. In addition, TDDFT calculations for Pheo with various functionals of B98 (22% HF exchange),³⁸ PBE0 (25% HF exchange),³⁹ BMK (42% HF exchange),⁴⁰ and BHandH (50% HF exchange)⁴¹ are also performed to investigate the effect of HF exchange within DFT functional.

In addition to the gas-phase calculations, we also perform TD-B3LYP/6-31+G(d,p) calculations for both Pheo and Chl in solvent, with implicit bulk solvent being taken into account using the polarizable continuum model (PCM) initially devised by Tomasi and co-workers^{42,43} combined with the solute cavity

defined by the united atom topological model (UAHF)⁴⁴ based on radii optimized for the HF/6-31G(d) level of theory. Since we are interested in the vertical excitation energies, the nonequilibrium solvation calculations are performed; i.e., the slow component of solvent reaction field established according to ground-state charge density will not be changed according to the excited-state charge density during the fast excitation process. Solvent models with different polarity such as water (H₂O, with dielectric constant $\epsilon = 78.39$), methanol (CH₃OH, $\epsilon = 32.63$), ethanol (CH₃CH₂OH, $\epsilon = 24.55$), and chloroform (CHCl₃, $\epsilon = 4.9$) are considered.

3. Results and Discussion

3.1. Optimized Ground-State Geometries. In general, the B3LYP/6-31G(d,p) optimized bond lengths of Pheo tend to be 0.014 Å longer on average than the X-ray crystal structures⁶ with a mean absolute deviation of 0.018 Å (see supporting data Table S1 of the Supporting Information). The slightly shorter bond lengths in X-ray crystal structures could be due to the condensed phase effect. Since the experimental bond lengths⁶ have an uncertainty of about 0.01 Å, such agreement between experimental and our B3LYP geometries is quite satisfactory. On the other hand, due to the lack of electron correlation, the HF/6-31G(d,p) method tends to predict somewhat shorter bond lengths and more “localized” (i.e., shorter) double bonds within the conjugated chlorin π -system as compared with the B3LYP/6-31G(d,p) method. This leads to smaller average deviation of 0.003 Å but evidently larger mean absolute deviation of 0.025 Å from X-ray structures.⁶ For example, the differences between two adjacent N2–C9 and N2–C6 bond lengths are 0.025, 0.024, and 0.102 Å from X-ray structure,⁶ B3LYP/6-31G(d,p), and HF/6-31G(d,p) geometries. Similarly, the respective differences between two adjacent C14–C15 and C15–C16 bond lengths is –0.002, 0.026, and 0.108 Å, with the HF geometries showing the largest bond length variation. It should be pointed out that similar effects of electron correlation on the geometry of highly symmetrical porphyrin and chlorin had also been observed previously.⁴⁶ However, the effects of unreasonable HF geometries on the excitation energies remain unclear. This could be revealed by a comparison with results based on B3LYP geometries. On a similar but smaller test system of pyrrole, further increasing the basis set from 6-31G(d,p) into 6-311G(d,p) and 6-311+G(d,p) in B3LYP calculations leads to bond lengths shortened slightly within 0.002 Å, suggesting converged geometry at the B3LYP/6-31G(d,p) level. As will be shown later, such unreasonable behavior of HF geometries may lead to too high excitation energies.

3.2. Effects of HF and B3LYP Geometries on Vertical Excitations. Table 1 lists the TD-B3LYP and ZINDO calculated excitation energies of Pheo in the gas phase using both the B3LYP and HF optimized geometries as mentioned above, along with the available experimental data in ethanol solvent^{2,3} and recent MRCI/DFT calculations.¹¹ For better comparison, we have included the same number of bright states (with oscillator strength > 0.1) and dark states (with oscillator strength ≤ 0.1). To estimate oscillator strengths from spectral integration of experimental absorption spectra, the molar extinction coefficients of 44500 M⁻¹cm⁻¹ for Pheo in ethanol at 667 nm and 111700 M⁻¹cm⁻¹ for Chl in methanol at 417.8 nm are used. For the visible Q_y and Q_x bands where several vibronic peaks exist, only the lowest energy (0,0) vibronic peak is integrated. Due to the strong overlapping between the B_x and B_y components, the total B-band oscillator strength is integrated in the 380–460 nm range and then partitioned approximately according to estimated intensities for the B_x and B_y components.

TABLE 1: Effects of B3LYP/6-31G(d,p) and HF/6-31G(d,p) Geometries on the Excitation Energies (eV, with Oscillator Strength in Parentheses) of Pheophorbide *a* Calculated within the TD-B3LYP/6-31+G(d,p) and ZINDO Methods

N	TD		ZINDO		MRCI/DFT ^a	expt ^b	nature
	B3LYP	HF	B3LYP	HF			
1	2.114 (0.18)	2.443 (0.17)	1.638 (0.24)	2.390 (0.17)	1.93 (0.28)	1.86 (0.28)	Q _y
2	2.308 (0.03)	2.585 (0.04)	2.214 (0.04)	2.847 (0.25)	2.40 (0.07)	2.33 (0.04)	Q _x
3	2.914 (0.00)	3.270 (0.02)	3.141 (0.00)	3.227 (0.00)	2.94 (0.04)	—	CT
					2.99 (0.42)		
4	3.147 (0.50)	3.359 (0.47)	3.077 (1.93)	3.424 (1.36)	3.17 (1.22)	3.04 (0.95)	B _y
5	3.193 (0.79)	3.490 (0.69)	3.296 (1.56)	3.621 (0.89)	3.25 (1.19)	3.14 (0.90)	B _x
6	3.280 (0.02)	3.875 (0.02)	3.859 (0.05)	4.007 (0.01)		—	CT
7	3.318 (0.00)	3.832 (0.02)	3.939 (0.04)	4.022 (0.00)		—	CT
8	3.529 (0.35)	3.468 (0.24)	3.461 (0.34)	3.753 (0.43)		3.36	η
9	3.690 (0.10)	3.947 (0.00)	3.952 (0.00)	4.031 (0.01)		—	CT
10	3.796 (0.43)	3.911 (0.24)	3.542 (0.24)	3.941 (0.23)		3.81	N

^a Taken from ref 11. ^b Experimental excitation energies read from refs 2 and 3 with oscillator strengths estimated by spectral integration.

It can be seen that, when the B3LYP geometries are used, both the TD-B3LYP and ZINDO calculated excitation energies for the Q_y, Q_x, B, and N bands agree quite well (mostly within 0.1 eV) with the experimental data^{2,3} and recent MRCI/DFT calculations.¹¹ The largest deviation is found for the lowest Q_y excited state, which is overestimated by about 0.25 eV within TD-B3LYP but underestimated by 0.2 eV within the ZINDO method as compared with experimental data.^{2,3} Note that an additional bright state around 2.99 eV is predicted by MRCI/DFT¹¹ but missed in both our TD-B3LYP and recent SAC-CI calculations,¹⁰ possibly due to the high double-excitation character of 45% and/or to the simplified molecular structure.¹¹ On the other hand, the experimentally estimated oscillator strengths are qualitatively reproduced by both TD-B3LYP and ZINDO calculations, with the TD-B3LYP predicted values being about 40% too small and the ZINDO predicted B bands being about 60% too strong. As will be shown later, the oscillator strengths can be enhanced by solvent effects, leading to much better agreement with experiment.

When the HF geometries of Pheo are used instead, the TD-B3LYP predicted excitation energies are evidently increased by more than 0.3 eV, especially for dark states 6 and 7. The ZINDO predicted excitation energies are also increased when the HF geometries are used, to a smaller extent of about 0.1 eV for dark states 6 and 7 but to a larger extent of more than 0.6 eV for the lowest Q_y and Q_x bands (excited states 1 and 2). Interestingly, all of the TD-B3LYP, ZINDO, and MRCI/DFT¹¹ methods predict the existence of dark state 3 slightly below (for TD-B3LYP and MRCI/DFT) or very close (for ZINDO) to the B bands around 3.0 eV, no matter what HF or B3LYP optimized geometries for Pheo are used. Such state is important since it may provide an internal conversion mechanism after B-band excitation of a single Pheo chromophore as an intermediate state. Similar dark states have already been observed experimentally for free-base and zinc tetratolylporphyrins.⁴⁵

Although TDDFT performs usually very well for valence excited states, it may have severe problems with the correct description of charge-transfer states of molecules exhibiting extended π -systems. Due to the vanishing overlapping between the MOs involved in the corresponding electronic transition, the oscillator strengths of CT states are usually very small and thus CT states are not easy to observe experimentally by absorption spectra. The excitation energies for CT states are usually drastically underestimated and do not exhibit the correct 1/*R* dependence along a charge-separation coordinate *R*, which fortunately can be recovered by inclusion of nonlocal HF exchange in the DFT exchange-correlation functional.²² In the

case of Pheo molecule, the singlet ¹(n, π^*) and ¹(π , π^*) CT states could be produced by electron transfer from electron lone pairs of N and O atoms to the chlorin π -system and from one pyrrole ring to another, respectively. As can be seen from Table 1, when the reasonable B3LYP geometries of Pheo are used, the TD-B3LYP predicted excitation energy of dark state 3 agree well with the ZINDO value. For dark states 6 and 7 the TD-B3LYP values are about 0.6 eV lower than the ZINDO values that are expected to be accurate. These results together with the near-zero oscillator strengths could be an indication of a strong CT-state nature of dark states 6 and 7. In a similar sense, the bright states 1, 4, 5, 8, and 10 do not show much CT-state character, since the oscillator strengths are quite large and the excitation energies of these states predicted by TD-B3LYP and ZINDO methods are quite close.

3.3. Nature of Singlet Excited States. To provide some insight into the nature of possible excited states, important frontier molecular orbitals (MO) of Pheo and Chl molecules at the B3LYP/6-31+G(d,p) level are shown in Figure 2. Among the six highest occupied molecular orbitals (HOMOs, 6 up to 1 in ascending energy order) of Pheo, 1 and 2 are π -orbitals delocalized over the whole tetrapyrrole ring with a small 1–2 gap of 0.2 eV, and both are energetically well-separated from other occupied MO 3 by more than 0.79 eV. The π -orbital 3 is mainly localized on pyrrole ring II, while the π -orbital 4 localized on ring I with substantial contribution from its vinyl (CH₂=CH-) substituent has a 3–4 gap of 0.4 eV. The n-orbital 5 is localized mainly on the carbonyl oxygen electron lone pair of ring V, while the π -orbital 6 is mainly localized on rings III and V. On the other hand, the four lowest unoccupied molecular orbitals (LUMOs, 1* up to 3*) are all π -orbitals delocalized over the whole tetrapyrrole ring, with a large HOMO–LUMO (i.e., 1–1*) gap of 2.43 eV. The orbital 4* consists mainly of the π^* -orbital of the vinyl substituent of ring I. Other higher LUMO levels seem not very important to the 10 lowest excited states of Pheo and thus are not shown. Except for the n-orbital (electron lone pair) 5, all other occupied MOs 6–1 show substantial overlapping with the delocalized LUMOs 1*–3*. This suggests that most transitions should be of *valence* excitation nature, though transitions from the somewhat localized π^* -orbitals 3, 4, and 6 are expected to have *partial* charge-transfer character. On the other hand, transitions from n-orbital 5 to π^* -orbital of 1*–3* should be of charge-transfer character due to near-zero orbital overlapping.

As can be seen from Figure 2, the shape and energy levels of HOMOs 1 and 2 as well as LUMOs 1* up to 4* of Chl are essentially the same as those of Pheo, due to very similar

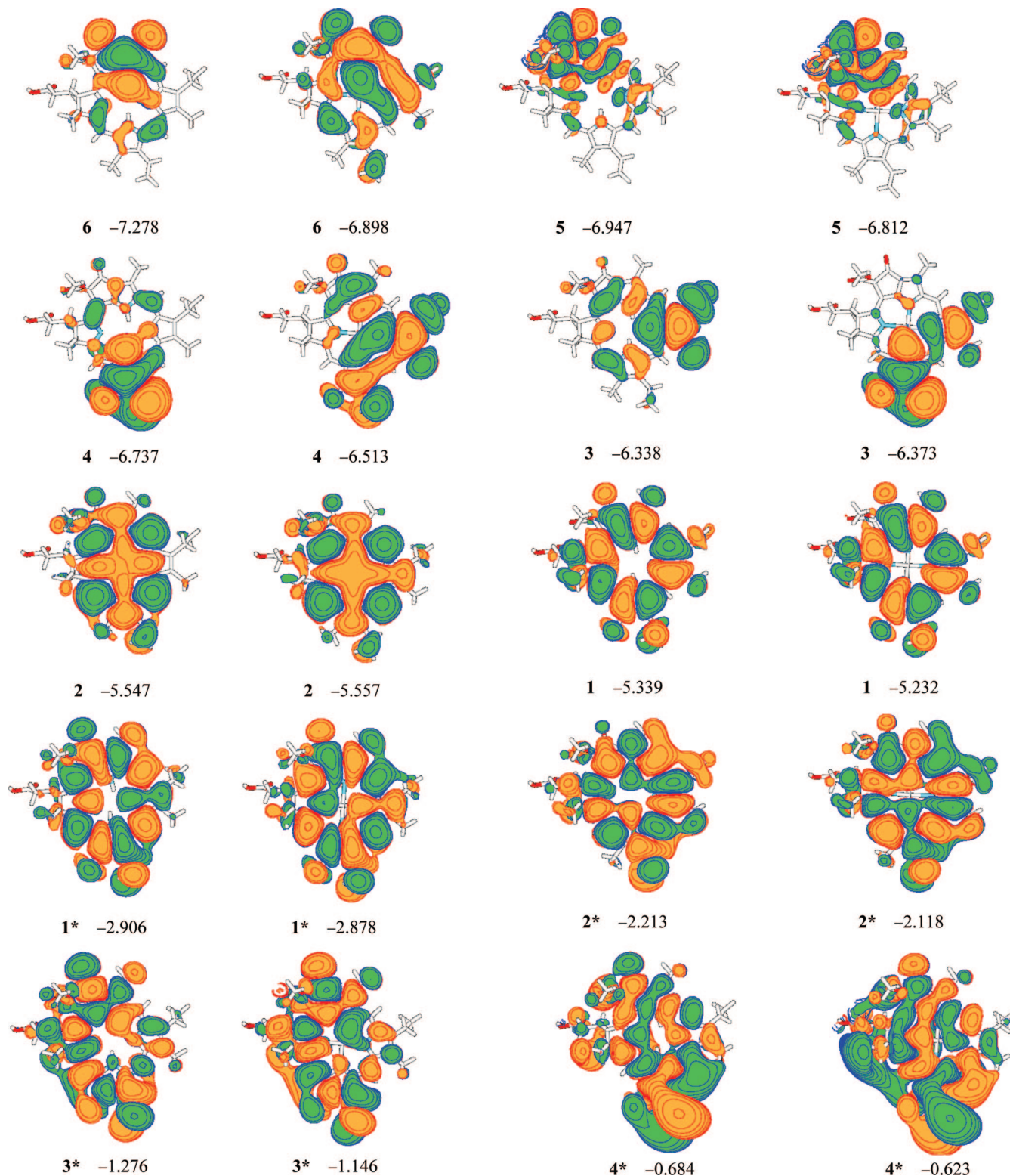


Figure 2. The B3LYP/6-31+G(d,p) calculated frontier orbital energies (eV) of the six highest occupied (6 up to 1 in ascending energy order) and four lowest unoccupied (1* up to 4*) molecular orbitals of pheophorbide *a* (from left to right, the first and third column of panels) and chlorophyllide *a* (from left to right, the second and fourth column of panels). Note that the HOMO (labeled as 1) orbitals are the 162nd and 157th doubly occupied orbitals, respectively. The plotting contour surface is chosen at electronic density of 0.005 au, with the positive and negative parts shown in yellow and green, respectively.

molecular structure. However, subtle differences do exist for some lower occupied orbitals due to central Mg substitution within Chl. First, now the π -orbital 3 in Chl is mainly localized on ring I with substantial contribution from its vinyl ($\text{CH}_2=\text{CH}$ -) substituent, while the π -orbital 4 is on pyrrole ring II with small contribution from ring I, which is thus on the *reverse* order of

Pheo. This leads to a similar energy level of orbital 3 in both Chl and Pheo, but the 3–4 gap of 0.14 eV in Chl is evidently smaller than that of 0.40 eV in Pheo. Second, the orbital levels of 5 and 6 in Chl are elevated by about 0.14 and 0.38 eV, respectively, leading to rather small 5–6 gap of 0.09 eV in Chl as compared with 0.33 eV in Pheo. Such subtle differences may

TABLE 2: Lowest Excitation Energies (E , eV, with Oscillator Strengths in Parentheses), the Angle between Transition Dipole and x -Axis (α , deg), and the Coefficients of Main Singly Excited Configurations (Greater than 0.15) Calculated at the TD-B3LYP/6-31+G(d,p) Level for Both Chl and Pheo Molecules in Gas Phase

N	state	Pheo			Chl			comments
		E (eV)	α	coefficients ^a	E (eV)	α	coefficients ^a	
1	π,π^*	2.114 (0.18)	-88	0.588 (1 \rightarrow 1*) -0.366 (2 \rightarrow 2*)	2.106 (0.24)	-87	0.598 (1 \rightarrow 1*) -0.306 (2 \rightarrow 2*)	Q_y
2	π,π^*	2.308 (0.03)	-10	0.564 (2 \rightarrow 1*) 0.397 (1 \rightarrow 2*)	2.286 (0.03)	-12	0.570 (2 \rightarrow 1*) 0.399 (1 \rightarrow 2*)	Q_x
3	π,π^*	2.914 (0.00)	28	0.679 (3 \rightarrow 1*)	3.112 (0.14)	-9	0.619 (4 \rightarrow 1*) -0.209 (1 \rightarrow 2*)	partial CT from ring II
4	π,π^*	3.147 (0.50)	60	0.449 (2 \rightarrow 2*) -0.263 (3 \rightarrow 2*) -0.227 (1 \rightarrow 2*) 0.171 (2 \rightarrow 3*) 0.159 (1 \rightarrow 1*)	3.284 (0.71)	-74	0.541 (2 \rightarrow 2*) 0.154 (1 \rightarrow 1*)	B_y
5	π,π^*	3.193 (0.79)	-30	0.427 (1 \rightarrow 2*) -0.227 (2 \rightarrow 1*) 0.204 (2 \rightarrow 2*) -0.189 (3 \rightarrow 2*)	3.124 (0.41)	13	0.422 (1 \rightarrow 2*) 0.273 (4 \rightarrow 1*) -0.224 (2 \rightarrow 1*) -0.172 (2 \rightarrow 2*)	B_x
6	n,π^*	3.280 (0.02)	-8	0.657 (5 \rightarrow 1*) 0.177 (5 \rightarrow 3*)	3.192 (0.04)	-4	0.647 (5 \rightarrow 1*)	CT from carbonyl
7	π,π^*	3.318 (0.00)	56	0.672 (4 \rightarrow 1*)	2.949 (0.02)	-87	0.677 (3 \rightarrow 1*)	CT from vinyl
8	π,π^*	3.529 (0.35)	-81	0.575 (3 \rightarrow 2*) 0.206 (2 \rightarrow 2*) 0.165 (2 \rightarrow 3*) 0.188 (1 \rightarrow 3*)	3.682 (0.01)	60	0.455 (4 \rightarrow 2*) 0.440 (3 \rightarrow 2*) 0.232 (1 \rightarrow 3*)	η for Pheo, partial CT from ring II
9	π,π^*	3.690 (0.11)	-46	0.629 (1 \rightarrow 3*)	3.697 (0.09)	-30	0.578 (1 \rightarrow 3*) -0.303 (3 \rightarrow 2*)	η for Chl, partial CT from ring II
10	π,π^*	3.796 (0.43)	65	0.580 (2 \rightarrow 3*) 0.181 (6 \rightarrow 1*) -0.164 (1 \rightarrow 4*)	3.897 (0.31)	76	0.545 (2 \rightarrow 3*) 0.347 (7 \rightarrow 1*) -0.180 (1 \rightarrow 4*)	N
11	π,π^*	3.845 (0.07)	-50	0.533 (6 \rightarrow 1*) -0.328 (8 \rightarrow 1*) -0.222 (7 \rightarrow 1*)	3.480 (0.14)	-19	0.655 (6 \rightarrow 1*)	η for Chl, CT from carbonyl
12	π,π^*	4.026 (0.03)	-43	0.550 (4 \rightarrow 2*) 0.276 (1 \rightarrow 4*) 0.206 (7 \rightarrow 1*)	3.831 (0.16)	-58	0.497 (4 \rightarrow 2*) -0.411 (3 \rightarrow 2*) -0.174 (1 \rightarrow 3*)	N, partial CT from ring I and II

^a (2 \rightarrow 1*) stands for the singly excited configuration from the second highest occupied orbital (HOMO) into the first lowest unoccupied orbital (LUMO), and so on. The LUMO levels are indicated by superscript. *The HOMO (labeled as 1) levels of Chl and Pheo are the 162nd and the 157th doubly occupied molecular orbitals.

change the nature of some excited states and lead to higher density of states for Chl, as will be shown later. It should also be pointed out that in both Pheo and Chl the 2-3 and 1*-2* orbital gaps are comparable (of about 0.8 eV), which may break down the validity of the traditional Gouterman four-orbital model^{19,20} (including orbitals 2 up to 2*). For the description of B bands and higher spectral region, it seems that at least five (3 up to 2* for Pheo) or six (4 up to 2* for Chl) orbitals are required.

Table 2 compares lowest excitation energies and oscillator strengths as well as the main excitation configurations (with the largest CI expansion coefficients greater than 0.15) calculated at the TD-B3LYP/6-31+G(d,p)//B3LYP/6-31G(d,p) level of theory for both Chl and Pheo molecules in the gas phase. On the basis of the main excitation configurations in Table 2 and the frontier MOs (Figure 2) as discussed above, we conclude that for both Chl and Pheo the two lowest excited states 1 and 2 (Q_y and Q_x bands polarized approximately in the y and x axes direction, respectively) are clearly of singlet $^1(\pi,\pi^*)$ valence-excited-state nature (with marked overlapping between the MOs involved in the excitation configurations), which are due to transitions from delocalized orbitals 1 and 2 into 1* and 2* and thus consistent with the traditional four-orbital model. The $^1(\pi,\pi^*)$ dark state 3 is mainly due to transition from the orbital localized on ring II (orbital 3 for Pheo and 4 for Chl) into delocalized orbital 1* thus possessing partial charge-transfer character, though the oscillator strength is somewhat enhanced in Chl due to mixing with more valence excitation (1 \rightarrow 2*). The higher bright states 4, 5 (strong B_x and B_y bands, respectively), and 10 (N band) are mainly of singlet $^1(\pi,\pi^*)$ valence-excited-state nature. The somewhat "bright" $^1(\pi,\pi^*)$ excited states 8 and 9 should be also valence-excited-state of partial CT nature, which could be related to the unclearly resolved η band of Pheo and Chl, respectively. Some excited states can be related to the excitation of substituent groups to the tetrapyrrole ring. The dark state 6 is related to the excitation of oxygen electron lone pair within the ring V carbonyl group into delocalized π^* orbitals over the tetrapyrrole ring (5 \rightarrow 1* transition), which is clearly a $^1(n,\pi^*)$ CT state. The $^1(\pi,\pi^*)$ dark state 7 is related to the excitation from somewhat localized π -orbital over vinyl and

ring I (orbital 4 for Pheo and 3 for Chl) into delocalized orbital 1* and thus is of partial CT nature. For Chl, two additional $^1(\pi,\pi^*)$ partial CT excited states 11 and 12 are also found within the energy range up to the experimentally observed N band (excited state 10), though the corresponding excited states of Pheo are somewhat high-lying in energy. Since both states are bright, they could also contribute to the observed η and N bands of Chl, respectively.

3.4. Effects of HF Exchange Percentage within DFT Functionals. To investigate the effects of the percentage of HF exchange within the DFT functional on the HOMO-LUMO gap of Pheo, single-point calculations using the 6-31+G(d,p) basis set are also performed at the B3LYP/6-31G(d,p) optimized Pheo geometries, with various existing DFT functionals of BP86, B98, PBE0, BMK, and BHandH (with 0, 22, 25, 42, and 50% HF exchange, respectively) as well as the traditional HF method (with 100% HF exchange). One may also decide to change the HF-exchange ratio within the same chosen functional further to explore the effects of HF exchange. However, since all the DFT functionals chosen here are gradient-corrected functionals of similar quality, a new choice with fixed functional form is not expected to change the overall trends.

As can be seen from Table 3, the HOMO energy level of Pheo decreases while the LUMO level increases gradually with the percentage (PE) of HF exchange within the DFT functionals. The resultant HOMO-LUMO gap (E_{HL} , eV) increases almost linearly with the PE of HF exchange within the DFT functional, approximately according to the equation: $E_{HL} = 1.633 + 4.10PE$. Compared with the lowest experimental excitation energy of 1.86 eV, it is obvious that only the HOMO-LUMO gap from DFT functionals with about 10% HF exchange can be a good estimation of the lowest excitation energy.

To estimate a reasonable energy for a possible CT state of Pheo, we have also calculated the vertical ionization potential (IP) and electron affinity (EA) at the B3LYP/6-31+G(d,p) level as 6.44 and 1.81 eV, respectively. As expected, the IP value is quite close to the negative HOMO level of 6.286 eV from HF calculations, while the EA value is badly underestimated by the negative LUMO level of 0.299 eV due to the lack of electron correlation. On the other hand, the negative HOMO and LUMO

TABLE 3: HOMO and LUMO Levels and HOMO–LUMO Gaps (E_{HL} , eV) of Pheophorbide *a* Predicted by Various DFT Functionals, as Well as the B3LYP Predicted Ionization Potential (IP, eV) and Electron Affinity (EA, eV)

	BP86	B3LYP	B98	PBE0	BMK	BHandH	HF	ZINDO
exact %	0	20	22	25	42	50	100	100
HOMO	−5.007	−5.333	−5.333	−5.497	−5.796	−5.850	−6.286	−6.449
LUMO	−3.374	−2.912	−2.830	−2.830	−2.449	−2.177	−0.299	−1.932
E_{HL}	1.633	2.422	2.503	2.667	3.347	3.674	5.987	4.517
IP		6.44						
EA		1.81						

TABLE 4: Effects of Different HF Exchange within DFT Functionals in TDDFT Method on the Excitation Energies (in eV) and Oscillator Strengths (in Parentheses) Using the Same B3LYP/6-31G(d,p) Ground-State Geometries of Pheophorbide *a*

<i>N</i>	BP86	B3LYP	PBE0	BMK	BHandH	expt ^a	nature
1	2.025 (0.15)	2.114 (0.18)	2.141 (0.19)	2.168 (0.20)	2.141 (0.22)	1.86 (0.28)	Q _y
2	2.105 (0.03)	2.308 (0.03)	2.362 (0.03)	2.471 (0.03)	2.490 (0.03)	2.33 (0.04)	Q _x
3	2.345 (0.00)	2.914 (0.00)	3.048 (0.01)	3.380 (0.37)	3.690 (0.32)	–	CT
4	2.785 (0.26)	3.147 (0.50)	3.241 (0.57)	3.439 (1.04)	3.478 (1.02)	3.04 (0.95)	B _y
5	2.880 (0.33)	3.193 (0.79)	3.273 (0.89)	3.496 (0.49)	3.571 (0.89)	3.14 (0.90)	B _x
6	2.379 (0.00)	3.280 (0.02)	3.397 (0.01)	3.677 (0.00)	4.027 (0.00)	–	CT
7	2.740 (0.03)	3.318 (0.00)	3.444 (0.01)	3.783 (0.02)	3.969 (0.02)	–	CT
8	3.264 (0.22)	3.529 (0.35)	3.652 (0.42)	3.944 (0.49)	4.134 (0.44)	3.36	η
9	2.941 (0.01)	3.690 (0.11)	3.836 (0.07)	4.181 (0.03)	4.346 (0.03)	–	η
10	3.301 (0.35)	3.796 (0.43)	3.944 (0.36)	4.310 (0.23)	4.576 (0.14)	3.81	N

^a Experimental excitation energies read from refs 2 and 3 with oscillator strengths estimated by spectral integration.

levels of 6.449 and 1.932 eV from semiempirical ZINDO calculations are quite good estimations of IP and EA values of Pheo, mainly due to the parametrization for the ZINDO method at the CIS level to reproduce some experimental electronic spectra.³⁷ If an average charge separation (*R*) of about 8 Å is assumed, which corresponds approximately to the center distance between two opposite pyrrole rings, we could estimate an CT excitation energy around 2.9 eV according to (EA – IP – 1/*R*). This value agrees well with the first dark state around 3 eV predicted by TD-B3LYP and ZINDO methods as discussed above.

Table 4 shows the effects of HF exchange percentage within different DFT functionals on the excitation energies and oscillator strengths of Pheo. It can be seen that the oscillator strength increases gradually with increasing HF exchange percentage from the BP86 to BHandH method. Compared with the oscillator strengths estimated from experimental spectra,^{2,3} the BP86 predicted oscillator strengths for the bright Q_y and B bands are more than 47% too small, which are evidently improved by other DFT functionals including 20–50% HF exchange. On the other hand, the excitation energies increase gradually with increasing HF exchange percentage, to less extent for the lowest excited states 1 (Q_y) and 2 (Q_x) but rapidly for higher excited states. As compared with the experimental data,^{2,3} the energy of the first excited state 1 (Q_y) is slightly overestimated by all DFT methods by about 0.2 eV. The experimental² energy of the second excited state 2 (Q_x) around 2.33 eV is well-reproduced (within 0.03 eV) by both B3LYP and PBE0 functionals with about 20–25% HF exchange, but is underestimated by 0.2 eV by BP86 without HF exchange and overestimated by about 0.13 eV by BMK and BHandH functionals with more than 42% HF exchange, respectively. Similarly, the experimental excitation energies² for higher bright states (with oscillator strength > 0.1) such as B bands around 3 eV are well-reproduced within 0.1 eV by B3LYP functional, but are underestimated by more than 0.26 eV by BP86 and overestimated by about 0.2 eV by PBE0 and even more by other functionals with increasing HF exchange percentage. Thus, it seems that higher HF exchange percentage may lead to higher excitation energies, with the B3LYP functional performing best

for valence excited states than other DFT functionals. Recently, the CAM-B3LYP functional was proposed⁴⁷ to overcome the problem of traditional DFT methods of tending to underestimate CT-state energies, and it is used to study CT states within porphyrins and chlorophylls.¹³ Within this functional, the B3LYP functional form is chosen with increasing HF exchange percentage gradually from 0.19 at short range to 0.65 at long range.⁴⁷ However, similar to the behavior of the BHandH functional with high HF percentage, the CAM-B3LYP functional tends to evidently overestimate the valence excitation energies above Q bands though the CT excited-state energies are elevated.¹³

As can also be seen from Table 4, the excitation energies of dark states (with oscillator strength < 0.1) 3, 6, 7, and 9 are underestimated by at least 0.8 eV by BP86 functional as compared with the ZINDO values based on B3LYP geometries as shown in Table 1, and are increased rapidly with increasing HF exchange percentage within other DFT functionals. This may suggest the strong charge-transfer character of these dark states. For the dark states 3 and 9 the B3LYP and PBE0 excitation energies agree well with ZINDO data, which are evidently overestimated by BHandH with 50% HF exchange. For dark states 6 and 7 the BMK functional with 42% HF exchange show the best agreement with ZINDO data. It thus may conclude that including 20–40% HF exchange in DFT functionals may improve the performance for intramolecular CT states, but more than 20% HF exchange in DFT functionals may gradually lower the performance for valence-excited states.

3.5. Solvent Effects Based on PCM Model. Table 5 shows the results of TD-B3LYP/6-31+G(d,p) calculations with the PCM solvation model for chloroform, ethanol, methanol, and water to account for the solvent effects on the electronic spectra of Pheo. Compared with the corresponding gas-phase calculations, all the ¹(π,π^*) excitation energies are *red*-shifted by about 10–120 meV, dependent on the detailed nature of excited states. For example, for the four lowest ¹(π,π^*) excited states of 1, 2 (Q_y and Q_x bands, respectively), 3, and 4 (B_y band) the spectral red shifts are relatively small of only 10–40 meV, while for the higher ¹(π,π^*) excited states of 5 (B_x band) and 7 with more CT character the shifts become large of 70–120 meV. The

TABLE 5: Excitation Energies (E , eV) and Oscillator Strengths (in Parentheses) as Well as Solvent-Induced Spectral Shifts (S , meV) of Pheophorbide a Calculated at the TD-B3LYP/6-31+G(d,p) Level with PCM Solvent Model

N	state nature	E			S				
		gas	ethanol	expt ^a	chloro form	ethanol	methanol	water	water ^b
1	Q _y	2.114 (0.18)	2.087 (0.28)	1.86 (0.28)	-25	-27	-25	-25	-27
2	Q _x	2.308 (0.03)	2.290 (0.06)	2.33 (0.04)	-10	-18	-18	-20	-39
3	CT	2.914 (0.00)	2.891 (0.00)	—	-26	-23	-20	-15	-39
5	B _x	3.193 (0.79)	3.075 (0.79)	3.04 (0.95)	-103	-118	-113	-117	-136
4	B _y	3.147 (0.50)	3.115 (0.93)	3.14 (0.90)	-34	-32	-27	-29	-36
7	CT	3.318 (0.00)	3.205 (0.04)	—	-72	-113	-113	-115	-136
8	η	3.529 (0.35)	3.489 (0.19)	3.36	-40	-39	-36	-33	-51
6	CT	3.280 (0.02)	3.497 (0.05)	—	126	216	220	224	735
9	η	3.690 (0.11)	3.609 (0.19)	—	-56	-81	-80	-81	-117
10	N	3.796 (0.43)	3.720 (0.46)	3.81	-58	-76	-75	-79	-129

^a Experimental excitation energies read from refs 2 and 3 with oscillator strengths estimated by spectral integration. ^b With one explicit H₂O H-bonding to the ring V carbonyl.

TABLE 6: Excitation Energies (E , eV, with Oscillator Strengths in Parentheses) and the Solvent-Induced Shifts (S , meV) of Chlorophyllide a Calculated at the TD-B3LYP/6-31+G(d,p) Level in Gas Phase and in Solvent within PCM Solvent Model

N	state nature	E			S				
		gas phase ^a	MeOH ^b	expt ^c	MeOH ^d	MeOH	MeOH ^b	water	water ^b
1	Q _y	2.106 (0.24)	2.050 (0.35)	1.88 (0.23)	-47	-51	-56	-50	-60
2	Q _x	2.286 (0.03)	2.167 (0.08)	2.31 (0.03)	-52	-88	-118	-97	-118
7	CT	2.949 (0.02)	2.854 (0.01)	—	-72	-72	-95	-72	-88
5	B _x	3.124 (0.41)	2.973 (0.44)	2.97 (1.36)	-109	-133	-150	-130	-153
3	CT	3.112 (0.14)	3.005 (0.04)	—	-60	-85	-107	-72	-108
4	B _y	3.284 (0.71)	3.128 (0.74)	3.13 (0.85)	-102	-141	-156	-144	-168
6	CT	3.192 (0.04)	3.483 (0.01)	—	325	326	291	279	339
9	η	3.697 (0.09)	3.528 (0.30)	3.37	-100	-128	-169	-118	-210
10	N	3.897 (0.31)	3.630 (0.32)	3.84	-129	-185	-266	-179	-265
12	N	3.831 (0.16)	3.692 (0.28)	—	-35	-48	-139	-37	-142
8	CT	3.682 (0.01)	3.796 (0.15)	—	-23	-37	114	-25	103
11	CT	3.480 (0.14)	3.896 (0.07)	—	-30	-10	415	-9	435

^a Without solvent molecule. ^b With both solvent–Mg coordination and explicit H-bonding to ring V carbonyl. ^c Experimental data read from ref 3 with the oscillator strengths estimated by spectral integration. ^d Without explicit solvent molecule.

strong B_x bands are red-shifted more strongly by about 80 meV than the strong Q_y bands in all solvents tested here. Due to stronger red shift for the B_x band, it becomes about 40 meV lower than the B_y band in energy, thus in the reverse order as compared with the gas-phase results. The ¹(π,π^*) excited state 8 (η band) is red-shifted by about 33–40 meV, while 9 and 10 are red-shifted more strongly by 56–80 meV. Different from the ¹(π,π^*) excited states, the ¹(n, π^*) CT state 6 is strongly blue-shifted by 224 meV in water, but by less extent in less polar solvents. To test the effect of explicit H-bonding with ring V carbonyl, we have also optimized the Pheo–H₂O H-bonding complex and utilize the PCM model to account for the remaining solvent effect. As can be seen from the last two columns of Table 5, a comparison with simple PCM model results shows that the explicit H-bonding to ring V carbonyl of Pheo together with PCM model may slightly enhance the red shift for ¹(π,π^*) excited states by about 20 meV, but leads to a very strong blue-shift of 735 meV for the ¹(n, π^*) state 6. As can also be seen from Table 5, the oscillator strengths in ethanol are evidently enhanced by more than 50% for the strong Q_y and B_y bands,^{2,3} but almost unchanged for the N band and even somewhat reduced for the η band of Pheo in ethanol. Taking the solvent effects (red-shifted and enhanced bands) into account, the predicted excitation energies and oscillator strengths now agree much better with experiments.^{2,3}

Table 6 shows the results of TD-B3LYP/6-31+G(d,p) calculations with the PCM model to account for the solvent effects of methanol and water on electronic transitions of Chl. Now the situation is somewhat more complicated since the

interaction between the oxygen electron lone pair with central Mg-ion is strong and explicit H-bonding to ring V carbonyl may also be considered. Thus, we have also optimized two kinds of Chl–solvent complex structures, both with explicit Mg–solvent coordination, but only one with explicit H-bonding to ring V carbonyl. The remaining solvent effects are accounted for by the PCM model.

As can be seen from Table 6, within the most sophisticated solvation model including both explicit Mg–solvent coordination and explicit H-bonding to ring V carbonyl of Chl, the spectral shifts induced by both methanol and water solvents are quite similar within 20 meV for the ¹(π,π^*) excited states. In methanol, the strong Q_y band of Chl is red-shifted by 56 meV, which is about 100 meV smaller than the red shifts for the B_y and B_x bands. Strong red shifts of 169, 266, and 139 meV are also found for the higher bright ¹(π,π^*) excited states of 9, 10, and 12. A comparison with experimental spectra suggests that the excited state 9 can be related to the observed η band, while both excited states 10 and 12 may contribute to the so-called N bands. Both the ¹(n, π^*) excited state 6 and ¹(π,π^*) states 11 are related to ring V carbonyl substituent and are strongly blue-shifted in methanol by 291 and 415 meV, respectively. In water solvent, such blue shifts of CT states 6 and 11 are slightly enhanced by 48 and 20 meV, respectively, possibly due to the stronger polarity. Evidently, the strong solvent effects must be included in the modeling and assignment of the electronic spectra of metalloporphyrins in general.

As can be seen from Table 6, compared with the results from simple PCM model, explicit Mg–solvent coordination together

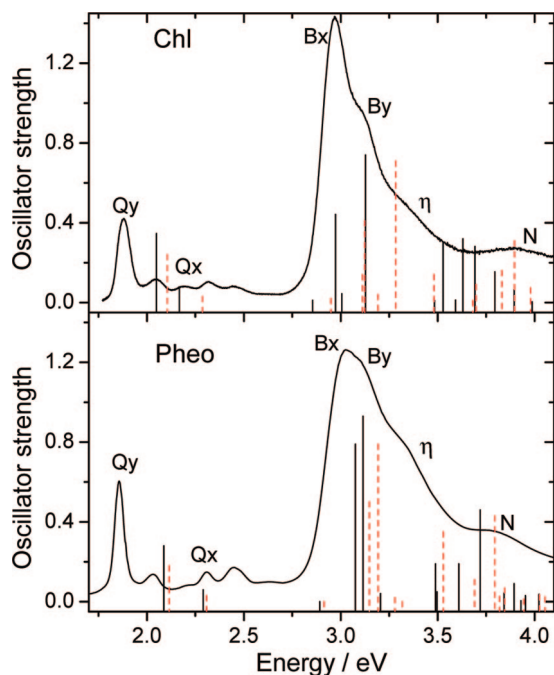


Figure 3. TDDFT predicted electronic absorption spectra in gas phase (in red dashed sticks) and in ethanol for pheophorbide *a* and in methanol for chlorophyllide *a* (in black solid sticks) within PCM model. The corresponding experimental spectra in solvents from refs 2 and 3 (in black solid lines) are also included for comparison.

with PCM model may slightly enhance the red shifts for $^1(\pi,\pi^*)$ excited states in methanol. Further inclusion of explicit H-bonding to ring V carbonyl may slightly enhance the red shifts for most low-lying $^1(\pi,\pi^*)$ excited states such as the strong Q and B bands by about 20 meV. For higher $^1(\pi,\pi^*)$ excited states the spectral shift pattern induced by explicit H-bonding are more complicated: the red shift for states 9 (η band), 10, and 12 (N band) are enhanced by 40–90 meV, but now the partial CT states 8 and 11 are blue-shifted! The $^1(n,\pi^*)$ state 6 is consistently strongly blue-shifted by about 300 meV in both methanol and water. However, the effects of the inclusion of explicit H-bonding are somewhat different on the blue shift of $^1(n,\pi^*)$ state 6 in methanol and water solvents: the blue shift becomes 35 meV smaller in methanol but 60 meV stronger in water.

The blue shift of $^1(n,\pi^*)$ transitions upon solvation is well-known for compounds containing electron lone pairs, which is mainly due to the weaker interaction with dielectric medium as the result of reduced local dipole along the lone pair direction after $^1(n,\pi^*)$ excitation.⁴⁸ It was shown that though explicit H-bonding itself may cause a red shift of $^1(n,\pi^*)$ state, further inclusion of dielectric solvent medium leads to a blue shift even about 0.2 eV larger than that obtained with only dielectric medium being considered.⁴⁸ The strong blue shifts in water for the carbonyl $^1(n,\pi^*)$ CT state 6 of both Pheo and Chl calculated in this work are consistent with the previous findings.⁴⁸ However, our results show that the inclusion of explicit H-bonding to ring V carbonyl may enhance (as in water) or reduce (as in methanol) the blue shift of $^1(n,\pi^*)$ state 6 in solvents. More test calculations seem to be needed to investigate the subtle effects of explicit H-bonding to compounds containing electron lone pairs.

3.6. Implications to the Assignment of Experimental Spectra. In Figure 3, the experimental absorption spectra of Pheo in ethanol and Chl in methanol are compared with our best theoretical calculations along with our new assignment

based on the calculated excitation energies, oscillator strengths and the nature of excited states. For both Chl and Pheo, the clearly resolved third vibronic peak may be assigned to the Q_x origin, in agreement with ref 8, but different from ref 9. In the near-ultraviolet region, the main peak and its first spectral shoulder of Chl are assigned to the B_x and B_y components, respectively, which is evidently different from the traditionally proposed assignment with two nearly degenerate B_x and B_y transitions for the main peak and with the first shoulder (η_1) related to the presence of ring V carbonyl.¹⁴ The resolved second spectral shoulder (η_2) is now labeled as the η band in our new assignment, which may be related to a partial CT transition from ring II (bright state 9) rather than the ring V carbonyl. For Pheo, the predicted B_y and B_x transitions are nearly degenerate, which is consistent with traditional assignment. The spectral shoulder next to the main peak is also labeled as an η band in our new assignment, which may also be related to partial CT transitions from ring II (bright states 8). For both the Pheo and Chl electronic spectra, the N band around 3.8 eV can be assigned to the bright $^1(\pi,\pi^*)$ excited state 10 with mainly valence rather than CT nature, which is different from the recent theoretical assignment¹³ that the N band of Chl is mainly due to CT excited state.

4. Conclusions

We have performed a detailed TDDFT analysis on electronic excitation spectra of Pheo and Chl, with PCM solvation model for bulk solvent and one explicit solvent molecule to a central Mg-ion to account for solvent effects. The main conclusions can be drawn as follows:

1. The B3LYP method leads to reasonable delocalized ground-state structures of both Pheo and Chl, while the HF method leads to too high excitation energies as the result of somewhat localized structure.
2. With increasing HF exchange percentage in DFT functionals, the predicted HOMO–LUMO gaps increase linearly, while the excitation energies increase gradually and even strongly for excited states with partial CT nature.
3. Solvent effects may shift most $^1(\pi,\pi^*)$ excitation energies to the red and increase the corresponding oscillator strengths of bright Q and B bands of Chl and Pheo, with the Q bands of Chl being the most sensitive. However, the $^1(n,\pi^*)$ excited state related to ring V carbonyl is strongly blue-shifted in solvents.
4. New assignment is given for the B and higher electronic absorption bands of Pheo and Chl.

Acknowledgment. We would like to acknowledge financial supports of the German Research Council (DFG) through Project MA 1356-10/1 and Collaborative Research Center (SFB450).

Supporting Information Available: Tables of the full comparison of bond lengths (without H) of Pheo between experimental data and HF and B3LYP calculations and of B3LYP optimized Cartesian coordinates of Pheo and Chl molecules as well as their solvent complexes. This information is available free of charge via the Internet at <http://pubs.acs.org>.

References and Notes

- (1) Hall, D. O.; Rao, K. K. *Photosyntheses*, 5th ed.; Cambridge University Press: Cambridge, U.K., 1995.
- (2) Hackbarth, S.; Ermilov, E. A.; Röder, B. *Opt. Commun.* **2005**, *248*, 295.
- (3) Du, H.; Fuh, R. A.; Li, J.; Corman, A.; Lindsey, J. S. *Photochem. Photobiol.* **1998**, *68*, 141.
- (4) Eichwurz, I.; Stiel, H.; Röder, B. *J. Photochem. Photobiol. B: Biology* **2000**, *54* (2–3), 194.

- (5) Wang, X. F.; Koyama, Y.; Nagae, H.; Wada, Y.; Sasaki, S.-i.; Tamiaki, H. *J. Phys. Chem. C* **2008**, *112*, 4418.
- (6) Fischer, M. S.; Templeton, D. H.; Zalkin, A.; Calvin, M. *J. Am. Chem. Soc.* **1972**, *94*, 3613.
- (7) Fragata, M.; Norden, B.; Kurusev, T. *Photochem. Photobiol.* **1988**, *47*, 133.
- (8) Houssier, C.; Sauer, K. *J. Am. Chem. Soc.* **1970**, *92*, 779.
- (9) Umetsu, M.; Wang, Z.-Y.; Kobayashi, M.; Nozawa, T. *Biochim. Biophys. Acta* **1999**, *1410*, 19.
- (10) Hasegawa, J.; Ozeki, Y.; Ohkawa, K.; Hada, M.; Nakatsuji, H. *J. Phys. Chem. B* **1998**, *102*, 1320.
- (11) Parusel, A. B. J.; Grimme, S. *J. Phys. Chem. B* **2000**, *104*, 5395.
- (12) Sundholm, D. *Chem. Phys. Lett.* **2000**, *317*, 545.
- (13) Cai, Z.-L.; Crossley, M. J.; Reimers, J. R.; Kobayashi, R.; Amos, R. D. *J. Phys. Chem. B* **2006**, *110*, 15624.
- (14) Petke, J. D.; Maggiora, G. M.; Shipmann, L.; Christoffersen, R. E. *Photochem. Photobiol.* **1979**, *30*, 203.
- (15) Sundholm, D. *Phys. Chem. Chem. Phys.* **2003**, *5*, 4265.
- (16) Parusel, A. B. J.; Grimme, S. *J. Porphyrins Phthalocyanines* **2001**, *5*, 225.
- (17) Linnanto, J.; Korppi-Tommola, J. *Phys. Chem. Chem. Phys.* **2006**, *8* (6), 663.
- (18) Vokacova, Z.; Burda, J. V. *J. Phys. Chem. A* **2007**, *111*, 5864.
- (19) Gouterman, M. *J. Mol. Spectrosc.* **1961**, *6*, 138.
- (20) Edwards, L.; Dolphin, D. H.; Gouterman, M.; Adler, A. D. *J. Mol. Spectrosc.* **1971**, *38*, 16.
- (21) Dreuw, A.; Head-Gordon, M. *J. Am. Chem. Soc.* **2004**, *126*, 4007.
- (22) Dreuw, A.; Head-Gordon, M. *Chem. Rev.* **2005**, *105*, 4009.
- (23) Zhu, H.; May, V.; Röder, B.; Renger, Th. *J. Chem. Phys.* **2008**, *128*, 154905.
- (24) Zhu, H.; May, V.; Röder, B.; El-Amine Madjet, M.; Renger, Th. *Chem. Phys. Lett.* **2007**, *444*, 118.
- (25) Zhu, H.; May, V.; Röder, B. *Chem. Phys.* **2008**, *351*, 117.
- (26) Frisch, M. J.; Trucks, G. W.; Schlegel, H. B.; Scuseria, G. E.; Robb, M. A.; Cheeseman, J. R.; Montgomery, J. A. Jr.; Vreven, T.; Kudin, K. N.; Burant, J. C.; Millam, J. M.; Iyengar, S. S.; Tomasi, J.; Barone, V.; Mennucci, B.; Cossi, M.; Scalmani, G.; Rega, N.; Petersson, G. A.; Nakatsuji, H.; Hada, M.; Ehara, M.; Toyota, K.; Fukuda, R.; Hasegawa, J.; Ishida, M.; Nakajima, T.; Honda, Y.; Kitao, O.; Nakai, H.; Klene, M.; Li, X.; Knox, J. E.; Hratchian, H. P.; Cross, J. B.; Bakken, V.; Adamo, C.; Jaramillo, J.; Gomperts, R.; Stratmann, R. E.; Yazyev, O.; Austin, A. J.; Cammi, R.; Pomelli, C.; Ochterski, J. W.; Ayala, P. Y.; Morokuma, K.; Voth, G. A.; Salvador, P.; Dannenberg, J. J.; Zakrzewski, V. G.; Dapprich, S.; Daniels, A. D.; Strain, M. C.; Farkas, O.; Malick, D. K.; Rabuck, A. D.; Raghavachari, K.; Foresman, J. B.; Ortiz, J. V.; Cui, Q.; Baboul, A. G.; Clifford, S.; Cioslowski, J.; Stefanov, B. B.; Liu, G.; Liashenko, A.; Piskorz, P.; Komaromi, I.; Martin, R. L.; Fox, D. J.; Keith, T.; Al-Laham, M. A.; Peng, C. Y.; Nanayakkara, A.; Challacombe, M.; Gill, P. M. W.; Johnson, B.; Chen, W.; Wong, M. W.; Gonzalez, C. Pople, J. A. *Gaussian 03*, Revision C.02; Gaussian: Wallingford, CT, 2004.
- (27) Becke, A. D. *J. Chem. Phys.* **1993**, *98*, 5648.
- (28) Lee, C.; Yang, W.; Parr, R. G. *Phys. Rev. B* **1988**, *37*, 785.
- (29) Hehre, W. J.; Ditchfield, R.; Pople, J. A. *J. Chem. Phys.* **1972**, *56*, 2257.
- (30) Frisch, M. J.; Pople, J. A.; Binkley, J. S. *J. Chem. Phys.* **1984**, *80*, 3265.
- (31) Roothan, C. C. *J. Rev. Mod. Phys.* **1951**, *23*, 69.
- (32) Casida, M. E.; Jamorski, C.; Casida, K. C.; Salahub, D. R. *J. Chem. Phys.* **1998**, *108*, 4439.
- (33) Bauernschmitt, R.; Ahlrichs, R. *Chem. Phys. Lett.* **1996**, *256*, 454.
- (34) Clark, T.; Chandrasekhar, J.; Spitznagel, G. W.; Schleyer, P. v. R. *J. Comput. Chem.* **1983**, *4*, 294.
- (35) Perdew, J. P. *Phys. Rev. B* **1986**, *33*, 8822.
- (36) Thompson, M. A.; Zerner, M. C. *J. Am. Chem. Soc.* **1991**, *113*, 8210.
- (37) Foresman, J. B.; Head-Gordon, M.; Pople, J. A.; Frisch, M. J. *J. Phys. Chem.* **1992**, *96*, 135.
- (38) Schmider, H. L.; Becke, A. D. *J. Chem. Phys.* **1998**, *108*, 9624.
- (39) Perdew, J. P.; Burke, K.; Ernzerhof, M. *Phys. Rev. Lett.* **1996**, *77*, 3865.
- (40) Boese, A. D.; Martin, J. M. L. *J. Chem. Phys.* **2004**, *121*, 3405.
- (41) Becke, A. D. *J. Chem. Phys.* **1993**, *98*, 1372.
- (42) Cossi, M.; Barone, V. *J. Chem. Phys.* **2001**, *115*, 4708.
- (43) Cancès, M. T.; Mennucci, B.; Tomasi, J. *J. Chem. Phys.* **1997**, *107*, 3032.
- (44) Barone, V.; Cossi, M.; Mennucci, B.; Tomasi, J. *J. Chem. Phys.* **1997**, *107*, 3210.
- (45) Schalk, O.; Brands, H.; Balaban, T. S.; Unterreiner, A. N. *J. Phys. Chem. A* **2008**, *112*, 1719.
- (46) Almlöf, J.; Fisher, T. H.; Gassman, P. G.; Ghosh, A.; Häser, M. *J. Phys. Chem.* **1993**, *97*, 10964.
- (47) Yanai, T.; Tew, D. P.; Handy, N. C. *Chem. Phys. Lett.* **2004**, *393*, 51.
- (48) Karelson, M.; Zerner, M. C. *J. Am. Chem. Soc.* **1990**, *112*, 9405.